Cooling dynamics of energized naphthalene and azulene radical cations

Jason W. L. Lee,[1] Mark H. Stockett,[2] Eleanor K. Ashworth,[3] José E. Navarro Navarrete,[2] Eva Gougoula,[1] Diksha Garg,[1] MingChao Ji,[2] Boxing Zhu,[2] Suvasthika Indrajith,[2] Nikolaj Klinkby,[4] Henning Zettergren,[2] Henning T. Schmidt,[2] and James N. Bull[3, a)]

[1)] *Deutsches Elektronen-Synchrotron DESY, Notkestr. 85, 22607 Hamburg, Germany*

[2)] *Department of Physics, Stockholm University, SE-10691 Stockholm, Sweden*

[3)] *School of Chemistry, Norwich Research Park, University of East Anglia, Norwich NR4 7TJ, United Kingdom*

[4)] *Department of Physics and Astronomy, Aarhus University, Aarhus 8000, Denmark*

Naphthalene and azulene are isomeric polycyclic aromatic hydrocarbon and are topical in the context of astrochemistry due to the recent discovery of substituted naphthalenes in the Taurus Molecular Cloud (TMC-1). Here, the thermal- and photo-induced isomerization, dissociation, and radiative cooling dynamics of energized naphthalene (Np^+) and azulene (Az^+) radical cations, occurring over the microsecond to seconds timescale, are investigated using a cryogenic electrostatic ion storage ring affording 'molecular cloud in a box' conditions. Measurement of the cooling dynamics and statistical dissociation kinetic energy release distributions, out to several seconds following hot ion formation, are consistent with establishment of a rapid (sub-microsecond) $Np^+ \rightleftharpoons Az^+$ quasi-equilibrium, and dissociation by C_2H_2-elimination proceeds predominately through Az^+ decomposition pathways. Simulations of the isomerization, dissociation, recurrent fluorescence, and infrared cooling dynamics using a coupled master equation combined with high-level potential energy surface calculations (CCSD(T)/cc-pVTZ), reproduce the trends in the experimental data. The data show that radiative cooling via recurrent fluorescence, predominately through the Np^+ $D_0 \leftarrow D_2$ transition, efficiently quenches dissociation for internal vibrational energies up to ≈1 eV above dissociation thresholds. These measurements support the suggestion that small PAH molecules, like naphthalene, may be more abundant in space than previously thought. The strategy presented in this work could be extended to fingerprint the cooling dynamics of other PAH ions for which isomerization is predicted to precede dissociation.

I. INTRODUCTION

Naphthalene and azulene (FIG. 1) are the simplest polycyclic aromatic hydrocarbons (PAHs) isomers and are the archetypal couple for PAH isomerization dynamics. PAHs are commonly generated in flames and incomplete combustion of organic material,[1,2] and are surmised to be ubiquitous in space.[3,4] Notably, more than 10% of interstellar carbon is thought to exist as PAHs,[5,6] and are conjectured to be major contributors to IR bands in astronomical observations, potentially including the so-called aromatic infrared bands (AIBs).[7–10] In the context of interstellar PAHs, naphthalene and derivatives are highly topical following the discovery of two isomers of cyanonaphthalene in TMC-1 through assignment of rotational lines, with an abundance six orders of magnitude higher than standard modeling predicted.[11] This discovery has, at long last, identified specific PAHs in space. Prior to this discovery, it was thought that PAHs with less than ca. 20 atoms would not radiatively stabilize following ionizing interactions;[12–14] clearly these models need revision and quantitative laboratory data for calibration.[15] Shortly after the discovery of the cyanonaphthalenes, the indene molecule was identified using similar methodology and found to be four orders of magnitude more abundant than modeling predicted.[16] In addition to neutral PAHs, charged forms are thought to control the ionization balance in molecular clouds,[17] influence protoplanetary ion-molecule chemistry, and are important sources of photoelectrons in the diffuse interstellar medium and the surface layers of protoplanetary disks.[18–20]

Following the first report of the thermal rearrangement of (neutral) azulene to naphthalene in 1947,[21] there have been numerous experimental studies on their light- and heat-induced interconversion – see Wentrup and co-workers[22] for a recent summary. Experiments on the radical cations of naphthalene (Np^+) and azulene (Az^+), and related PAH cations, have concluded that photoactivation is followed by rapid internal conversion (picoseconds) to recover the ground electronic state.[23–26] Significantly, for Np^+ and Az^+, because isomerization barriers are lower than dissociation barriers, isomerization reaction rates are higher and, therefore, energized Az^+ or Np^+ may (over certain internal energy

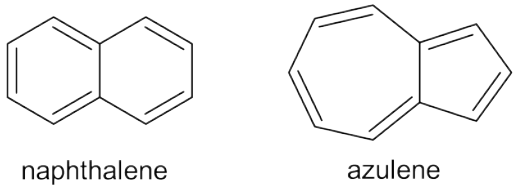

FIG. 1. Molecular structures of the $C_{10}H_8$ isomers naphthalene and azulene. The radical cations are denoted Np^+ and Az^+, respectively.

a)Electronic mail: james.bull@uea.ac.uk

windows) statistically dissociate *via* common intermediates and mechanisms.[23,27–32] These dynamics have been partially confirmed through calculation of potential energy surfaces and kinetic modeling of the isomerization and dissociation pathway,[33–36] although further characterizations on the competition between cooling pathways are required.

The cooling dynamics of energized PAH ions occurring over extended timescales (e.g., milliseconds to seconds) can be probed using ion storage devices, such as the approach implemented by Bernard et al.,[37] in which the slow thermal decay of activated Np^+ was studied in a room-temperature electrostatic ion storage ring. The study highlighted the importance of both infrared (IR) radiative cooling, occurring through vibrational transitions,[38] and recurrent fluorescence (RF), corresponding to photon emission from thermally-populated electronic states via inverse internal conversion.[39,40] A subsequent work by Saito et al.[41] directly observed RF for the $D_0 \leftarrow D_2$ transition in energized Np^+. In a recent contribution, some of the present authors used DESIREE (Double ElectroStatic Ion Ring ExpEriment) at Stockholm University to study 1-cyanonaphthalene radical cations (1-CNN^+) and infer the importance of RF in the cooling dynamics relevant in astrochemical environments,[15] and also to propose that RF-assisted cooling of PAHs may be more common than previously thought.

Due to the importance of naphthalene and azulene as fundamental PAH isomers and because of their relevance in astrochemistry as precursors in 'bottom-up' growth mechanisms for larger PAHs,[42] the present report seeks to: (i) measure cooling rates for energized Np^+ and Az^+ under 'molecular cloud in a box' conditions,[43,44] (ii) provide an assessment of the isomerization between Np^+ and Az^+, based on measuring kinetic energy release (KER) distributions associated with dissociation and monitoring time-dependent cooling dynamics following thermal- and photo-activation, and (iii) assess the importance of RF in the cooling dynamics of Np^+ and Az^+, and imply the preponderance of these species in space. While room temperature storage ring experiments can access 'slow' dynamics, occurring up to milliseconds after ion formation or activation, they cannot unequivocally probe the 'ultraslow' processes occurring over milliseconds to seconds.[38] Furthermore, the present experiments are the first conducted under conditions mimicking cold ($T = 10 - 20$ K) molecular clouds.

II. METHODS

A. Experimental

The cooling dynamics of energized Np^+ and Az^+ were studied at the DESIREE infrastructure (FIG. 2). Np^+ or Az^+ were generated through sublimation of the parent powder (Sigma-Aldrich, >99%) in a resistively heated

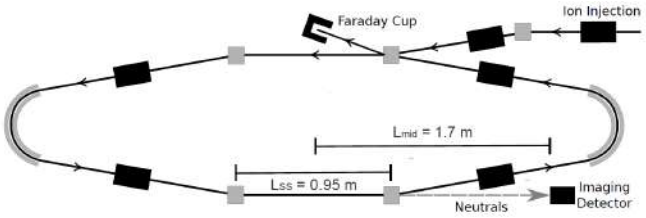

FIG. 2. Schematic diagram of the symmetric ion storage ring in DESIREE at Stockholm University. Cryogenic cooling of the ring to $T \approx 13$ K gives a residual gas density of $\approx 10^4$ cm^{-3} (mostly H_2).[45] Neutral products formed in the lower straight section follow the dashed line and are counted with the Imaging Detector.

oven coupled to an electron cyclotron resonance (ECR, Pantechnik Monogan) ion source with helium support gas. Cations extracted from the source were accelerated to 34 keV kinetic energy, mass selected (m/z=128) using a 90° bending magnet, and injected into the storage ring (orbit period $\approx 38\,\mu$s). The total ion transit time from formation to storage was $\approx 100\,\mu$s and $\approx 5\times10^4$ ions were injected each cycle (beam storage lifetime ≈ 500 s). After ion injection into the storage ring, neutral fragments formed in the lower straight section of the ring (see FIG. 2) impact on the position sensitive 'Imaging Detector'.[46] The detector consists of ultra-high dynamic range micro-channel plates (MCPs, Photonis), suitable for high count rates at cryogenic temperatures, coupled with a phosphor screen. Ion images were recorded through a vacuum window using a CMOS camera (Photon Focus MV1-D2048) with 1.1 ms exposures every 2.5 ms. The images are time-stamped and synchronized with the storage cycle. In separate single-pass experiments, ion images providing KER distributions were recorded using a 0.5 mm aperture inserted before the straight section of the storage ring to reduce the smearing of the neutral distributions due to the spatial extent of the beam.

Photo-induced experiments were performed by merging the stored ion beam with light (11 μJ $pulse^{-1}$, 250 Hz, unfocussed) from an EKSPLA NT-242 optical parametric oscillator (OPO) laser in a colinear geometry in the upper straight section of the ring. The irradiation wavelengths at 415 nm (Np^+) and 425 nm (Az^+) were selected based on high absorption cross-sections in cold electronic spectra[47,48] and because of high laser fluence in this wavelength range.

B. Theoretical

1. Potential energy surfaces

Calculations of the isomerization and dissociation (mainly C_2H_2 elimination) potential energy surfaces (PESs) for Np^+ and Az^+ involved optimizing the min-

imum energy structures and transition states at the ωB97X-D/cc-pVTZ level of theory, followed by single-point energy calculations at the CCSD(T)/cc-pVTZ level of theory using Gaussian 16.B01.[49–52] Initial structures were taken from Ref. 34.

2. Isomerization and dissociation

Isomerization between Np^+ and Az^+ and dissociation as C_2H_2-elimination (and H-elimination for Np^+) were modeled using an RRKM (Rice–Ramsperger–Kassel–Marcus) equation

What's the difference between E and E prime?

$$k(E) = \frac{\int_0^E \rho_t(E')dE'}{h\rho_r(E)} \quad (1)$$

where E is the vibrational energy, and ρ_r and ρ_t are level densities for the reactant and transition state, respectively, and h is Planck's constant. On our relative energy scale, $E = 0$ corresponds to the ground state vibrational energy of Np^+. For all other structures, the level density starts (is non-zero) at the structure's ground state energy.

3. Recurrent fluorescence

Recurrent fluorescence (RF), which is otherwise known as Poincaré fluorescence, corresponds to fluorescence emission from thermally populated electronic states.[40] The rate coefficient for RF, k_{RF}, was modeled using the expression:

$$k_{RF}(E) = A^{RF}\frac{\rho(E - h\nu_{el})}{\rho(E)} \quad (2)$$

where ρ is a density of states and ν_{el} is the electronic transition energy. The electronic Einstein coefficients, A^{RF}, were calculated by

$$A^{RF} = \frac{2\pi\nu_{el}^2 e^2}{\epsilon_0 m_e c^3} f \quad (3)$$

where f is the oscillator strength taken from Franck-Condon-Herzberg-Teller simulations at the LC-ωHPBE/cc-pVTZ level of theory.[53,54] Briefly, the low-lying electronic transitions of Np^+ have been determined using photoelectron and matrix-isolation spectroscopies,[47,55] with the first excited state ($^2B_{1u}$) at 0.73 eV and the second excited state ($^2B_{2g}$) between 1.93 and 1.84 eV. The first excited state is symmetry forbidden in absorption spectroscopy. Adjusting the experimental absorption value for vertical fluorescence transition energy based on our DFT calculations gives 1.66 eV. This value is in good agreement with the recurrent fluorescence spectrum for Np^+ in Ref. 41. Spectroscopic investigations on Az^+ are more limited, although a photoelectron spectroscopy study of thermally-evaporated azulene has reported the first two transitions at 1.09 and 2.66 eV.[56] For our RF simulations, we used the estimated fluorescence vertical transition energies combined with our calculated oscillator strengths at $f = 0.094$ for $D_2 \leftarrow D_0$ in Np^+ and $f = 1.7 \times 10^{-3}$ and 1.2×10^{-2} for $D_1 \leftarrow D_0$ and $D_2 \leftarrow D_0$ in Az^+, respectively.

4. IR emission

Infrared emission (vibrational cooling) rate coefficient, k_{IR}, for Np^+ and Az^+ were modeled assuming the simple harmonic cascade (SHC) approximation:[38]

$$k_{IR}(E) = \sum_s k_s = \sum_s A_s^{IR} \sum_{v=1}^{v \le E/h\nu_s} \frac{\rho(E - vh\nu_s)}{\rho(E)} \quad (4)$$

where v is the vibrational quantum number, $h\nu_s$ is the transition energy, and A_s^{IR} is the Einstein coefficient for vibrational mode s. The performance of this model has been discussed elsewhere,[38,57] but generally reproduces experimental data within a factor of two.

C. Master equation propagation

The time-dependent vibrational energy distribution, $g(E,t)$, initially normalized such that $\int g(E, t = 0)dE = 1$, was propagated according to the Master equation

$$\begin{aligned}\frac{d}{dt}g(E,t) = &-(k_{d,tot}(E) + k_{iso}(E))g(E,t) + \overline{k}_{iso}(E)\overline{g}(E,t) \\ &\sum_s [k_s(E - h\nu_s)g(E + h\nu_s, t) - k_s(E)g(E,t)] \\ &+k_{RF}(E + h\nu_{el})g(E + h\nu_{el}, t) - k_{RF}(E)g(E,t).\end{aligned} \quad (5)$$

In this expression, the first terms in parentheses describe depletion of the ion population by unimolecular dissociation (i.e., C_2H_2- and H-elimination) and isomerization, where the total dissociation rate coefficient is the sum of the rate coefficients for the various product channels, $k_{d,tot} = \sum_P k_{d,P}$. The next term is incoming population from the other isomer, with the overbars indicating the other isomer. The first term in brackets corresponds to $v + 1 \rightarrow v$ vibrational emission from levels above E, while the second is associated with $v \rightarrow v - 1$ emission to levels below E. The final two terms describe RF. The time step dt was chosen to match the experimental data, with 32 extra points prior to the first experimental time bin to allow for the ion transit time from the ion source to the storage ring. The simulated dissociation rate for a given product channel P is given by

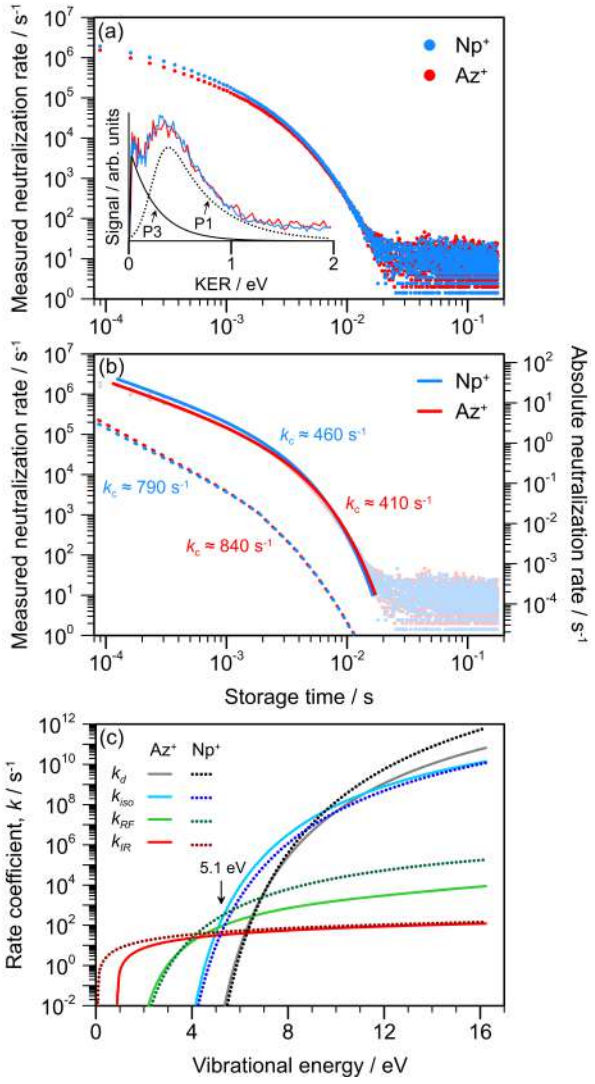

FIG. 3. Spontaneous neutralization of energized Np^+ and Az^+ produced in an ECR source: (a) measured neutralization rate with ion storage time, including single-pass kinetic energy release (KER) distributions associated with C_2H_2-elimination are shown in the inset, (b) fit of neutralization rate to EQN 6 and total simulated neutralization rate for Np^+ and Az^+ precursors, (c) simulated rate coefficients for C_2H_2-elimination (k_d), isomerization (k_{iso}), recurrent fluorescence (k_{RF}), and infrared cooling (k_{IR}). The average vibrational energy of the nascent ion ensembles is estimated at ≈5.1 eV, as indicated in (c). For (a) and (b), given rates are instrument dependent; absolute rates according EQN 9 are indicated on the right-hand vertical abscissa. In (c), the computed k_{RF} data are consistent with values in Ref. 41. Note the logarithmic scales on vertical and some horizontal abscissas.

$$\Gamma_P(t) = \int k_{d,P}(E) g(E,t) dE. \quad (6)$$

III. RESULTS AND DISCUSSION

A. Spontaneous cooling dynamics

Measured neutralization rates, $R(t)$, for Np^+ and Az^+ generated in the ECR source are shown in FIG. 3a. These data are averaged over a large number of injection and storage cycles, and have a similar shape to those reported for other PAH cations.[58,59] Intriguingly, the measured storage time dependence of the neutralization rates for the two precursor ions are near identical. In terms of the underlying physics of the neutralization rate curves, during the first $\approx 10^{-3}$ s after ion injection, the neutralization rate follows a power law trend, $R(t) \propto t^{-1}$, due to the broad distribution of internal energies, $[g(E,t)]$, of the ions and the rapid variation of the dissociation rate coefficient, $k_d(E)$, with E.[60] After a critical time (k_c^{-1}), the dissociation rate is quenched by competition with radiative cooling (RF and IR),[61] resulting in a dissociation rate with approximate time dependence

$$R(t) = r_0 t^{-1} e^{-k_c t} \quad (7)$$

where r_0 is signal amplitude. The solid curves in FIG. 3b are fits of EQN 7 to the $R(t)$ data for $t > 5 \times 10^{-4}$ s. Extracted values of k_c are $\approx 460\,s^{-1}$ (Np^+) and $\approx 410\,s^{-1}$ (Az^+) and are comparable with those for 1-CNN^+ ($k_c = 300 \pm 20\,s^{-1}$)[15,62] and other larger PAH cations.[58,59,63] Significantly, the k_c values for precursor Np^+ and Az^+ (as well as the cooling profiles) are similar, indicating similar dissociation and cooling dynamics, i.e., a common mechanism, over the fitted timescale. Application of the alternative fitting model

$$R(t) = r_0 t^{-\alpha} e^{-k_c t} \quad (8)$$

returned values of $\approx 500\,s^{-1}$ for both ions, with values of α slightly less than unity. Deviation of α from unity (EQN 7) is attributed to a finite width internal energy distribution,[37,64] with $\alpha \approx 0$ corresponding to exponential-like decay of ions with a narrow and well-defined internal energy distribution. We return to discussing α values for the photo-induced neutralisation data.

The $R(t)$ data presented in FIG. 3 are relative data that depend on instrumental conditions. They can be converted to absolute rates, $\Gamma(t)$, using the expression

$$\Gamma(t) = \frac{f^2 q_e}{N_{cyc} \eta_{det} G I_{avg}} R(t) \quad (9)$$

where $f = 23.87$ kHz is the revolution frequency of the stored ions, q_e is the electron charge, $I_{avg} = 300$ pA (124 pA for Az^+) is the measured beam current at the end of the storage cycle, $N_{cyc} = 213,177$ (226,712 for Az^+) is the number of cycles, $\eta_{det} = 0.4$ is the detector

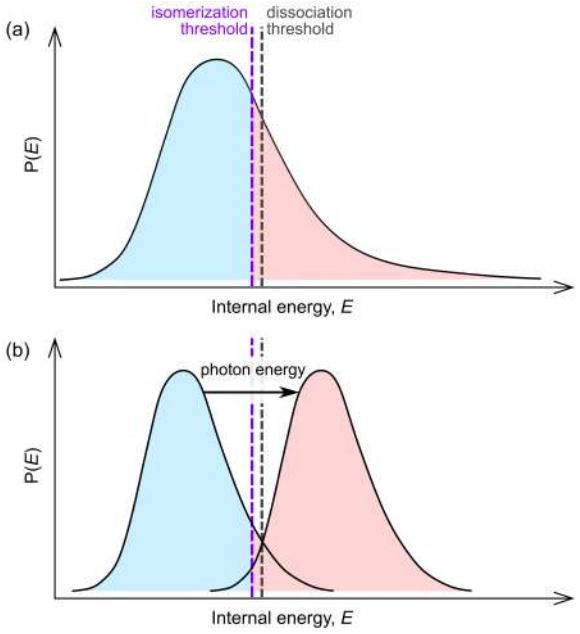

FIG. 4. Schematic illustrations of ion internal energy distributions, $[g(E,t)]$: (a) nascent Np^+ and Az^+ produced in the ECR source. Many of the ions are produced with high internal energies (red) in excess of the isomerization and dissociation threshold; these ions are subject to a competition between isomerization, dissociation, and cooling through RF and IR emission. A fraction of the nascent ions have internal energies lower than isomerization and dissociation thresholds (shaded blue), and may cool through IR and RF emission, with any destruction through dissociation. The ions in the blue shaded region retain the precursor isomer structure and are those that become increasingly probed with ion storage time in the photo-induced experiments. (b) The blue population corresponds to stored ions that have cooled to some degree. This population contains both Np^+ and Az^+, but will be enriched in the precursor ion because of the blue fraction of the population in (a). Upon absorption of a visible photon (photo-induced experiments), the average internal energy is raised above the isomerization and dissociation thresholds.

efficiency, and $G = 0.11$ is the fraction of the storage ring witnessed by the detector.

Kinetic energy release (KER) distributions recorded by imaging neutral products formed during the first 100 μs after ions were injected into the ring are shown in the inset in FIG. 3a. The KER distributions associated with decomposition of Np^+ and Az^+ are essentially identical, providing some evidence that dissociation (and interlinked cooling dynamics) proceed through common mechanisms. Furthermore, there is little change in shape of the KER distribution over the first 10 ms of ion storage, indicating that a quasi-statistical $Np^+ \rightleftharpoons Az^+$ equilibrium is promptly established after ion generation in the ECR source. We use the term 'quasi-statistical' because the internal energy distribution is presumably broad with a substantial fraction of the ions possessing internal energy in excess of isomerization and dissociation thresholds (FIG. 4). The KER distributions in FIG. 3a, inset, have a double-peaked structure with maxima at ≈0.05 eV and ≈0.4 eV, which differs from the Boltzmann-like KER distribution (peak maximum at ≈0.05 eV) recently measured for 1-CNN^+ using the same methodology.[15] Thus, there are multiple neutral formation (dissociation) pathways for the Np^+–Az^+ couple, which are not active for 1-CNN^+. As discussed below, these KER distributions are consistent with isomerization in concert with dissociation.

B. Potential energy surfaces

To link the Np^+ and Az^+ cooling measurements with PESs for isomerization and dissociation, we recomputed the most probable PESs reported in the 2006 work by Dyakov *et al.*[34], who used RRKM theory to explore the importance of each pathway with internal energy. For isomerization, the norcaradiene-vinylidene (or Dewar-Becker) isomerization mechanism[65,66] (FIG. 5a) is a two-step rearrangement, proceeding *via* a metastable, hydrogen-shifted naphthalene intermediate (species **6**). Conversely, the bicyclobutane isomerization mechanism[67] (FIG. 5b) is more complex, involving four transition states and three intermediates (species **3**, **4**, and **5**), although requires slightly lower activation energy. For dissociation leading to C_2H_2-elimination (FIG. 6a), the decomposition of Np^+ involves hydrogen shifts, followed by ring opening, forming the phenylacetylene cation (**P3**), which is the highest point (i.e., asymptotic) along the PES (4.75 eV, relative to Np^+). On the other hand, there are two feasible C_2H_2-elimination channels for Az^+ (FIG. 6b), both of which have a slightly lower limiting barrier at 4.72 eV. The barrier height to **TS1_20** is much larger than to **TS1_18**, making the latter the more likely forwards pathway. However, the reverse pathway starting from **P1** likely favors the route through **TS20_21**, as the barrier is significantly lower than to **TS19_21** (0.13 eV and 0.84 eV, respectively).

While experiments and supporting theoretical studies have demonstrated that C_2H_2- and H-elimination are the lowest energy dissociation pathways for the Np^+–Az^+ couple,[30,34,36] with approximately equal branching ratio at low excess internal energies (e.g., 1 eV above threshold), the imaging detector in DESIREE is insensitive to H atoms,[59] so the KER distributions should reflect C_2H_2 formation. H-loss, if present, would be spread widely over the detector due to the low mass of H, and would be indistinguishable from background in the KER image. On the other hand, our master equation simulations combine all of these isomerization and dissociation PESs as well as an H-elimination channel (see SI). It is worth noting a RRKM study on Np^+–Az^+ isomerization and dissociation dynamics used PESs calculated with the (becoming obsolete) B3LYP density functional,[36] however, our cou-

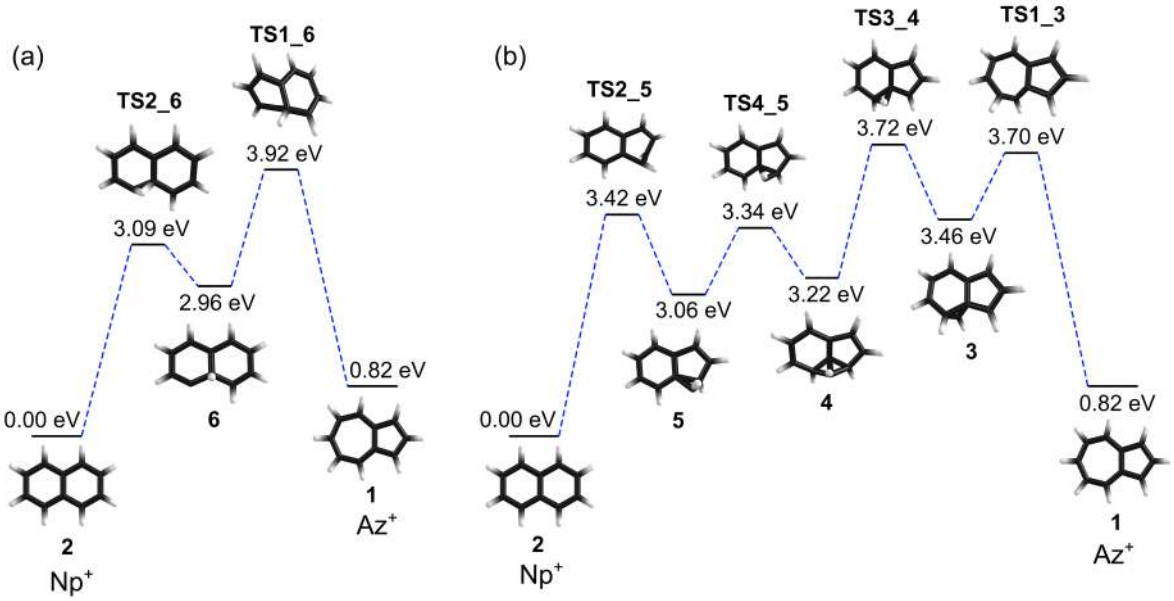

FIG. 5. Potential energy surfaces (CCSD(T)/cc-pVTZ) for Np^+ and Az^+ isomerization: (a) norcaradiene-vinylidene mechanism, (b) bicyclobutane mechanism. All energies are relative to Np^+. Labeling convention for the structures follows Ref. 34.

pled cluster PESs are in closer agreement with those in the Dyakov et al.[34] study, which employed the more robust G3(MP2,CC) method.

Returning to the KER distributions shown inset in FIG. 3a, we assigned the peak at ≈0.05 eV in the KER distribution to Np^+-dissociation yielding **P3** since the C_2H_2-elimination pathway is asymptotic in relative energy. The KER peak centred at ≈0.4 eV is assigned to dissociation from Az^+ yielding **P1** where kinetic energy associated with dissociation is portioned between the two fragments and internal vibrational excitation due to intramolecular vibrational energy redistribution concerted with bond scission.

C. Master equation simulations

A key result from the spontaneous neutralization data is that 'low energy' dissociation (i.e., up to several eV above the dissociation threshold) from either Np^+ or Az^+ occurs through common pathways because the Np^+–Az^+ isomerization barriers are lower than those for C_2H_2-elimination.[23,27–31] To understand the competition and interlink between isomerization, dissociation, and radiative cooling, we performed master equation simulations. The computed rates, using EQNS 1-4, the molecular structures and energies in FIGS 5 & 6, the vibrational frequencies tabulated in the Supplementary Material, are shown in FIG. 3c. The total C_2H_2-elimination rate (EQN 6) from a simulation assuming initial vibrational energy distributions following Boltzmann statistics with temperatures T = 1970 K for both isomers are shown in FIG. 3b. This temperature was chosen to match that found for previous experiments with 1-CNN^+ using the same ion source.[15] The initial temperature of T = 1970 K corresponds to an average internal energy of ≈5.1 eV, which is above the isomerization and dissociation barriers. Returning to FIG. 3c, in accord with the Dyakov RRKM study,[34,35] there is an internal-energy-dependent branching between the two C_2H_2-elimination channels. The dissociation channel producing **P3** in FIG. 6a is important at low internal energies (<5.2 eV), while the channel producing **P1**, in FIG. 6b (red), becomes more important after the 'turnover region' at ≈5.2 eV. At internal energies greater than ≈9.5 eV, the branching ratio for the **P3** channel begins to increase slightly, while the ratio for the **P1** channel begins to decrease (this decrease being greater than the corresponding increase in species **P3**). At our initial simulated temperature corresponding to ≈5.1 eV of internal energy, H-elimination and C_2H_2-elimination have roughly equal probability, with a 75%:25% branching between **P3** and **P1** products for C_2H_2-elimination. This C_2H_2-elimination channel branching is consistent with the 70%:30% (±10% uncertainty) determined from a fit of the single-pass KER distributions (dashed lines in FIG. 3a, inset).

D. Radiative cooling

The simulations in FIG. 3c indicate that RF cooling has the largest rate constant in the 4–5 eV internal energy range, with Np^+ being more efficient at RF than Az^+. This energy range spans UV absorption bands in

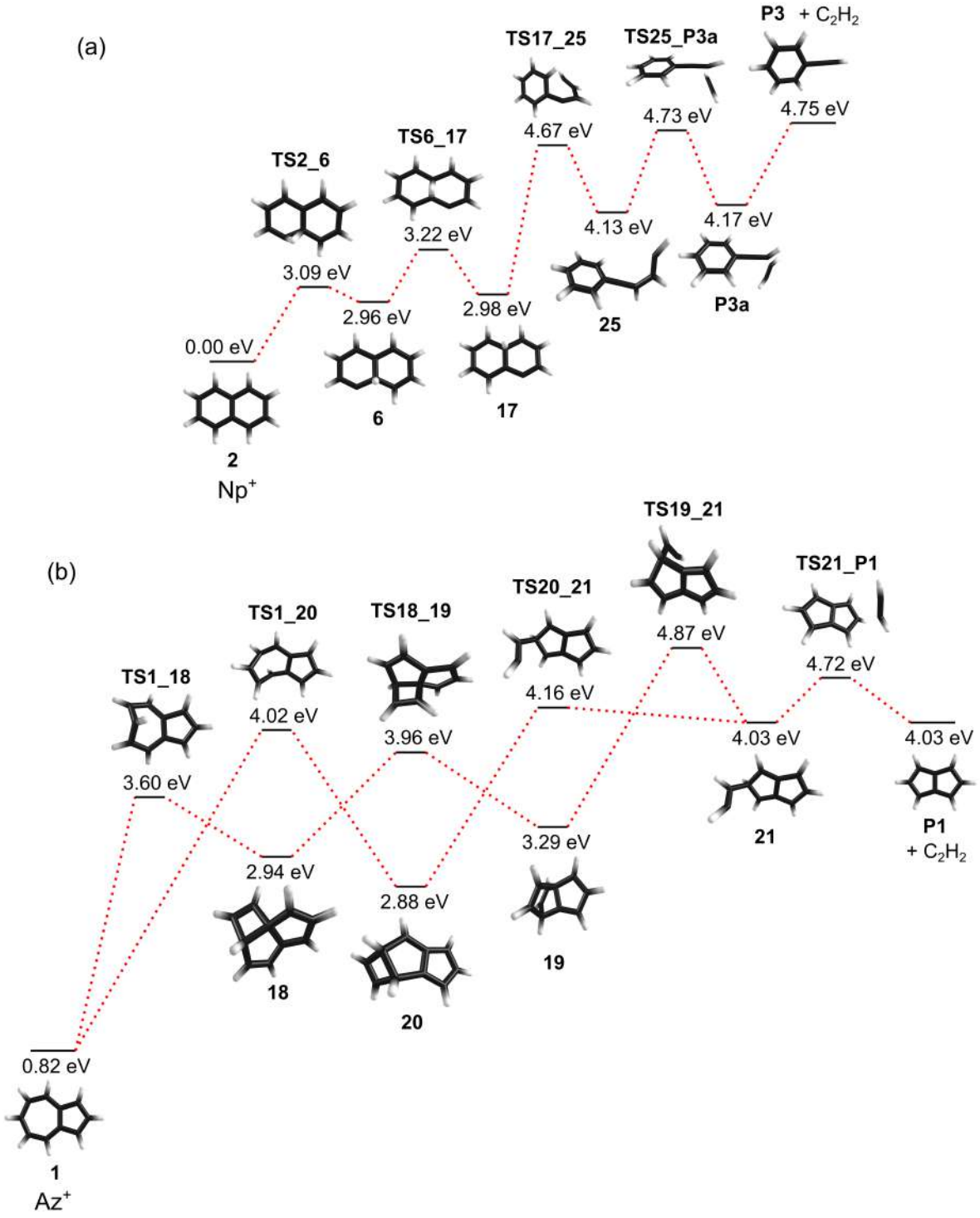

FIG. 6. Potential energy surfaces (CCSD(T)/cc-pVTZ) for dissociation (C_2H_2-elimination) from Np^+ and Az^+: (a) from Np^+ forming the phenylacetylene cation (**P3**), (b) from Az^+ forming the pentalene cation (**P1**). All energies are relative to Np^+. Labeling convention for the structures follows Ref. 34.

I suggest a x coordinate scale. And keep same linear scale.

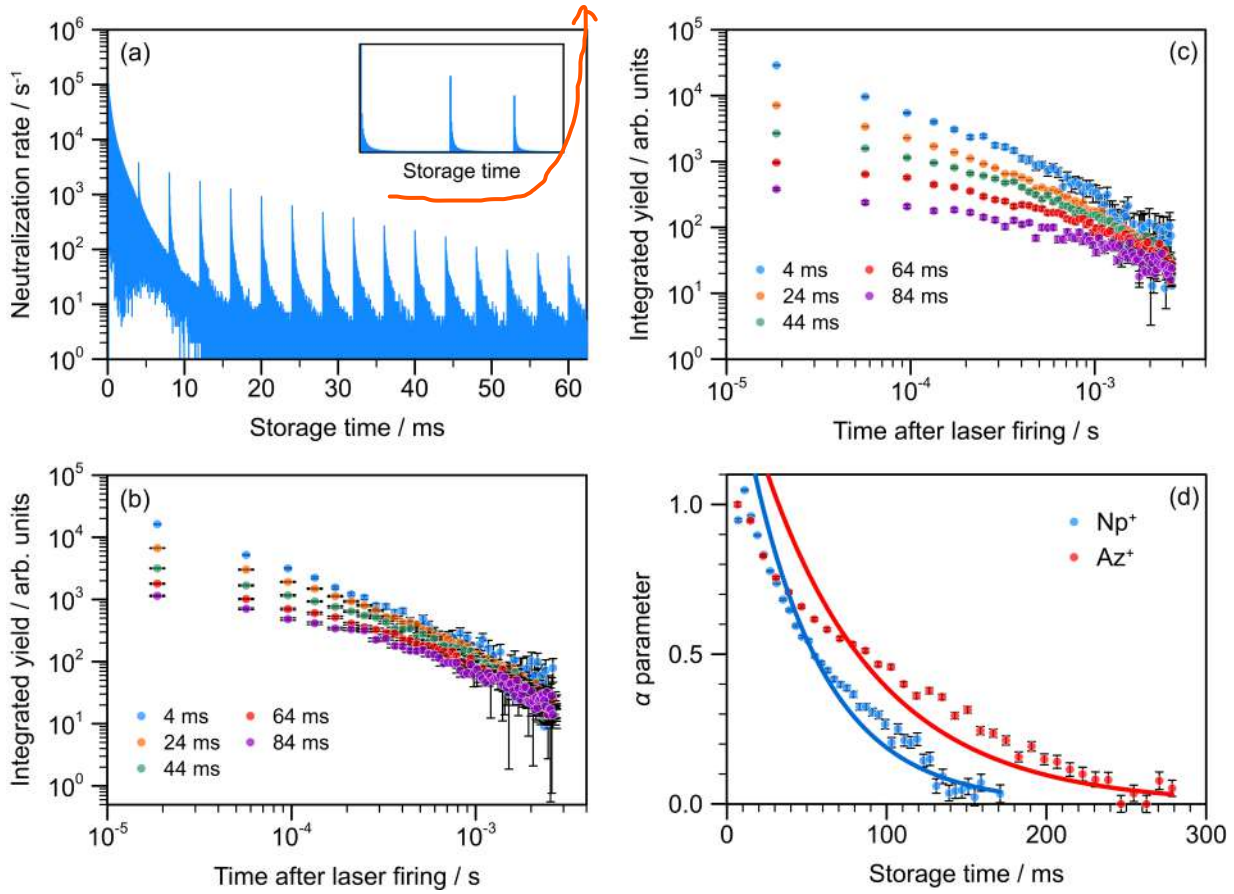

FIG. 7. Photo-induced neutralization of Np^+ and Az^+: (a) Example neutralization rate curve for Np^+ showing the first 15 laser irradiations using 415 nm light. (b) Background-corrected neutralization rates for five selected laser irradiations of source-heated Np^+. (c) Background-corrected neutralization rates for five selected laser irradiations of source-heated Az^+. (d) Values of fitted parameter α for the Np^+ and Az^+ irradiated cooling profiles. Exponential decay fits are included as a guide.

why it's exponential decay?

both ions. For internal energies below ≈4 eV, cooling is dominated by IR emission. The computed cooling rates for RF and IR are comparable with those determined for 1-CNN^+,[15] although RF cooling is slightly less efficient for Np^+ compared with 1-CNN^+ for vibrational energies <6 eV. The reduced rate of RF for Np^+, even though the oscillator strength $f = 0.094$ is substantially larger than $f = 0.011$ for 1-CNN^+, is because of the higher RF transition energy for Np^+ at ≈1.6 eV compared with the calculated value of 1.10 eV for 1-CNN^+. It is worth noting that our simulated RF rates for Np^+ are similar to those reported by Saito et al.[41].

Fits of the simulated neutralization curves to EQN 7, shown in FIG. 3b, returned k_c values of ≈790 s^{-1} for Np^+ and ≈840 s^{-1} for Az^+, which are 1.7–2-fold larger than the fitted values for the experimental data. This would indicate that the quenching of dissociation by radiative cooling is slightly overestimated by the model. Interestingly, the simulated absolute neutralization rates shown in FIG. 3b are about an order of magnitude lower than the (absolute) experimental data. We have applied similar master equation simulation methodology to describe the spontaneous cooling profiles for other PAH cations and found better agreement between absolute experimental rates, although these systems were not complicated by isomerization dynamics or multiple dissociation pathways.[15,58,59] Potential reasons for the difference in absolute rates in this work include: (i) the simulations assume a Boltzmann distribution with some average temperature; however, the true nascent ion temperature distribution may differ and have a different shape on the low temperature side, e.g. see Ref. 41 for an alternative internal energy distribution (although the distribution will be ion source and instrument specific), and (ii) the PESs for dissociation are complicated – our simulations considered only the lowest energy pathways for isomerization and elimination of C_2H_2, while theory has predicted several other pathways that may be cumulative.[34,36] Still, we conclude that the simulations are able to reasonably reproduce the experimental trends.

E. Photo-induced cooling dynamics

In addition to monitoring spontaneous neutralization of energized Np^+ and Az^+, we performed photo-induced neutralization experiments for which stored ions were irradiated at 415 nm (Np^+) or 425 nm (Az^+) every 4 ms. One may think of the photo-induced experiment as depositing a known amount of energy, 3.0 eV for Np^+ and 2.9 eV for Az^+, into the cooling ensemble (since internal conversion dynamics are fast compared with all other dynamics occurring on the ground state) – see FIG. 4b. The photo-induced cooling profile, averaged over many storage cycles, associated with the first 15 of the laser irradiations for Np^+ is shown in FIG. 7a. The inset shows the photo-induced responses corrected for the spontaneous neutralization background (i.e., no laser). Integrated neutralization yields as a function of time after laser firing for five selected ions storage times are shown in FIG. 7b (Np^+) and FIG. 7c (Az^+). These data were fit with the expression

$$At^{-\alpha}e^{-k_c t}. \tag{10}$$

In these fits, k_c was fixed to the value 460 s^{-1}, obtained from the spontaneous decay measurements. Values of α obtained from fits of EQN 10 are given in FIG. 7d, revealing an exponential-like decrease in magnitude with ion storage time, due to cooling and narrowing of the vibrational energy distribution. Significantly, while the two precursor ions gave similar values of α for short ion storage times (e.g., 0–50 ms), they start to deviate for longer ion storage times, indicating distinct cooling dynamics. Our interpretation is that, as the ion ensemble cools, the vibrational energy distribution illustrated in FIG. 4a evolves into the situation illustrated in FIG. 4b. Specifically, as the ion ensemble cools, many of the energized ions possessing energy in excess of the ionization and dissociation threshold are lost through dissociation, leaving the cooler part of the ion ensemble enriched in the precursor isomer. The deviatation of the trend in α, thus, reflects differences in radiative cooling (RF and IR) between the two precursor ions. Because α values for Np^+ have a steeper decrease with ion storage time than for Az^+, we conclude that RF cooling is more efficient for Np^+. This conclusion is consistent with both the fitted experimental k_c values in FIG. 3b (slightly larger for Np^+) and the simulations in FIG. 3c, where for $E > 3$ eV the computed k_{RF} value for Np^+ is larger than that for Az^+.

IV. ASTROCHEMICAL SIGNIFICANCE

For several decades, PAHs have been thought to be ubiquitous in the Interstellar Medium and to dominate the IR emission bands observed by astronomers at wavelengths coincident with PAH vibrational transition energies.[5,68–70] Interestingly, the AIBs only show small variations across astrochemical environments,[71] leading to the conclusion that these environments contain either a common subset of PAHs,[72] or a high diversity of PAHs that result in the same average spectrum.[73] These emission bands are ubiquitous in the universe, observed across many astrochemical environments, including the galactic interstellar medium, planetary nebulae, star forming regions, and other galaxies.[74,75] However, because they cannot be used to identify specific molecular species, it is desirable to have experimental characterizations of the cooling dynamics and IR emission properties of prototype PAHs. The conventional wisdom was that PAHs possessing less than ca. 20 atoms would not possess the ability to radiatively stabilize in space and would decompose.[12–14] However, the discovery of indene and two isomers of cyanonaphthalene in TMC-1 challenges this hypothesis.[11,16] Intriguingly, the observed abundances of the cyanonaphthalenes are six orders of magnitude higher than could be explained by standard astrochemical modeling involving growth mechanisms assuming a 'bottom-up' model from naphthalene. One hypothesis put forward by McGuire *et al.*[11] to explain the high abundance of CNN in TMC-1 is that a larger-than-expected amount of naphthalene was inherited from the diffuse interstellar medium at early stages of cloud formation. RF-enhanced stability of naphthalene is consistent with this hypothesis. As detailed in our recent study on 1-CNN^+,[15] part of the abundance discrepancy is likely because the destruction rate assumed in the model is too high; the model considered radiative stabilization effectuated by only IR emission, not by faster RF cooling, which is known to occur for Np^+.[41]

lives Despite isolated PAHs in space spending most of their live as an internally cold molecule, a key requirement for a PAH to be carrier of IR bands is that they it must survive any rare instances of collisional (thermal) heating such as from shock waves, and photo-induced heating (e.g., UV absorption or 13.6 eV H-ionization radiation in photodissociation regions). Photoresilience requires the molecule to liberate energy, i.e., radiative cooling, in a manner that suppresses dissociation. As shown in this work, while some fraction of energized Np^+ and Az^+ dissociate, RF leads to an appreciable fraction becoming stabilized (i.e., dissociation is suppressed). Thus, in accord with our recent study on 1-CNN^+, we reaffirm that RF is important for radiative stabilization of small PAHs, and that 'bottom-up' PAH growth models, like that assumed for cyanonaphtalene growth,[11] are likely astrochemical pathways. To help place the importance of radiative cooling into context, we plot ion survival probability with internal energy in FIG. 8. While dissociation thresholds are ≈4.8 eV, our simulations predict a near 100% survival rate of ions with internal vibrational energy < 5.8 eV, with a small fraction of ions surviving with internal energies up to ≈7 eV. Because the ionization potential of neutral naphthaene is 8.144±0.001 eV[76] and Np^+ can withstand < 5.8 eV of vibrational energy,

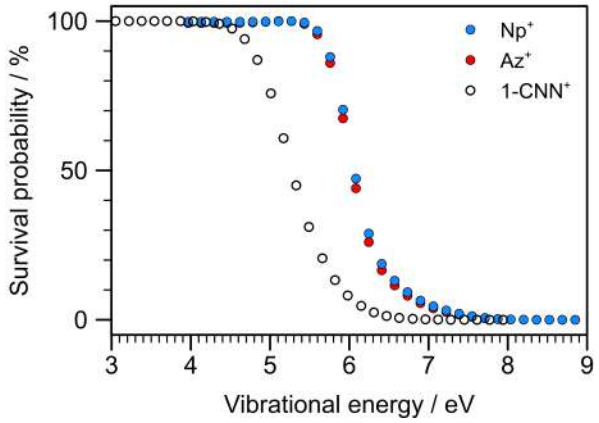

FIG. 8. Ion survival probability with internal energy from the master equation simulations. Data for 1-CNN^+ are taken from Ref. 15. The higher survival probability for Np^+–Az^+ compared with 1-CNN^+ over the 5–8 eV range is attributed to higher dissociation thresholds in the former.

neutral naphthalene molecules should retain their organic backbone following ionization by 13.6 eV H-ionization radiation. In contrast, the survival probability curve for 1-CNN^+ is shifted to ≈1 eV lower vibrational energy due to a lower dissociation threshold of ≈3 eV.[77] This is consistent with the iPEPICO results from West et al.[30], which show no appreciable fragmentation of naphthalene below 15 eV photon energies, although these experiments sampled shorter times after ionization than the present experiments and they may be subject to a kinetic shift.

Azulene has not been detected in space by the same radioastronomy surveys that identified CNN and indene.[11] While this may be partially due to the low dipole moment of azulene, it is also consistent with the present results showing that Az^+ excited by 5-7 eV converts to Np^+, and is then stabilized by RF. This process, and the equivalent one in the neutrals, would enrich naphthalene *vs* azulene.

V. CONCLUSIONS

This work has demonstrated that a rapid quasi-equilibrium, which precedes molecular decomposition, is established between Np^+ and Az^+ species generated in a thermal source. The measurements, which are supported by statistical modeling, provide characterization of the radiative cooling and associated dynamics over timescales relevant to the ions present in certain astrochemical environments. Access to these ultraslow timescales is afforded by conducting experiments under 'molecular cloud in a box' conditions. Master equation simulations are able to reproduce the radiative cooling properties of the ions and demonstrate that RF is the dominant non-destructive cooling mechanism. In accord with a recent study on cyanonaphthalene cations by some of the present authors,[15] we reaffirm that RF cooling: (i) is an important radiative cooling mechanism, (ii) is an important process for the photoresilience of small PAHs in space, and (iii) helps to account for the anomalous observed abundances of small PAHs in TMC-1 compared with predications from astrochemical models.

Although Np^+ and Az^+ are the 'simplest' PAH cations, in many regards, they represent the most complex PAH system studied at DESIREE so far, due to clear signatures for a competition between isomerization, dissociation, and radiative cooling (through RF and IR). For Np^+ and Az^+, this complexity is because isomerization barriers are lower than dissociation barriers. Similar situations may exist for a range of other PAH systems,[78–80] including ring-expanded *vs* ring-methylated PAHs, and PAHs containing an azulene-like moiety with an extended and a contracted ring.[77] Specific examples include radical cations of the anthracene-phenanthrene couple and the related $C_{13}H_9N^+$ system,[81–83] and isomers of pyrene and coronene.[84,85] Also of note, is that similar isomerization dynamics, particularly with hydrogen-shifts, may be common for PAHs with varying degrees of dehydrogenation.[78]

The methodology applied in this work, involving generating and storing hot radical cations and probing their spontaneous thermal and photo-induced cooling dynamics, can readily be extended to many of the systems noted above. However, future experiments, ideally, would focus on photo-induced cooling dynamics, for either open or closed shell ions, as a function of excitation wavelength, starting with internally-cold ions. The appeal of photo-induced experiments is the ability to deliver a precise amount of energy, provided that excitation is followed by prompt internal conversion to recover the ground electronic state (usually picoseconds in isolated PAHs)[23–26] and that ensuing intramolecular energy redistribution is rapid. Such experiments might best be conducted using a new electrospray ionization source available at DESIREE that incorporates a cryogenic pre-trap to cool ions before they are injection into the storage ring. This pre-cooling provides an internal energy distribution more similar to FIG. 4b, thereby avoiding waiting for hot ions produced in thermal sources to cool. For Np^+ and Az^+, provided they could be satisfactorily generated through electrospray ionization, this approach should provide near-pure ensembles of each isomer, avoiding the complications associated with coexisting isomers at the start of each ion storage cycle. For pure isomer ensembles, measurement of KER distributions as a function of excitation energy would provide a rigorous probe of PES barriers to isomerization and calibration of the master equation simulation methodology currently used to model cooling dynamics.

injected

SUPPLEMENTARY MATERIAL

The Supplementary Material contains details on: analysis methods for the kinetic energy release distributions,

theoretical methods for rate coefficient calculations, theoretical methods for PES calculations, calculated vibrational frequencies, and optimized geometries.

DATA AVAILABILITY

The data that support the findings of this study are available from the corresponding author and DESIREE facility upon reasonable request.

ACKNOWLEDGMENTS

Funding was provided by the Swedish Foundation for International Cooperation in Research and Higher Education (STINT) Grant for Internationalisation programme (PT2017-7328 to MHS and JNB), and an EPSRC New Investigator Award (EP/W018691 to JNB). JWLL acknowledges financial support from the Helmholtz-ERC Recognition Award (ERC-RA-0043) of the Helmholtz Association (HGF). EKA thanks the University of East Anglia for doctoral studentship. Electronic structure calculations were carried out on the High Performance Computing Cluster supported by the Research and Specialist Computing Support service at the University of East Anglia. We acknowledge the DESIREE infrastructure for provisioning of facilities and experimental support, and thank the operators and technical staff. The DESIREE infrastructure receives funding from the Swedish Research Council under the Grant numbers 2017-00621 and 2021-00155. This article is based upon work from COST Action CA18212 – Molecular Dynamics in the GAS phase (MD-GAS), supported by COST (European Cooperation in Science and Technology).

AUTHOR CONTRIBUTIONS

This work was based on a beamtime application prepared by JWLL, MHS, and JNB. JWL, MHS, JENN, EG, DG, MCJ, BZ, SI, and JNB participated in experimental data acquisition. HZ and HTS managed the DESIREE facility. Analysis of experimental data was performed by JENN, MHS, EKA, NK, and JNB. RRKM and master equation simulations were performed by MHS. Electronic structure calculations were performed by EKA and JNB. The manuscript was prepared by JNB with assistance from MHS and EKA, and was discussed by all authors.

CONFLICTS OF INTEREST

The authors have no conflicts to disclose.

REFERENCES

[1]G. Liu, Z. Niu, D. V. Niekerk, J. Xue, and L. Zheng, in *Reviews of Environmental Contamination and Toxicology* (Springer New York, 2008) pp. 1–28.
[2]M. Howsam and K. C. Jones, in *The Handbook of Environmental Chemistry* (Springer Berlin Heidelberg, 1998) pp. 137–174.
[3]T. Henning and F. Salama, Science **282**, 2204 (1998).
[4]A. G. G. M. Tielens, Rev. Mod. Phys. **85**, 1021 (2013).
[5]A. G. G. M. Tielens, Ann. Rev. Astron. Astrophys. **46**, 289 (2008).
[6]E. Peeters, Proc. Int. Astron. Union **7**, 149 (2011).
[7]G. Lagache, H. Dole, J.-L. Puget, P. G. Perez-Gonzalez, E. L. Floc'h, G. H. Rieke, C. Papovich, E. Egami, A. Alonso-Herrero, C. W. Engelbracht, K. D. Gordon, K. A. Misselt, and J. E. Morrison, Astrophys. J. Supp. Ser. **154**, 112 (2004).
[8]J. D. T. Smith, B. T. Draine, D. A. Dale, J. Moustakas, J. R. C. Kennicutt, G. Helou, L. Armus, H. Roussel, K. Sheth, G. J. Bendo, B. A. Buckalew, D. Calzetti, C. W. Engelbracht, K. D. Gordon, D. J. Hollenbach, A. Li, S. Malhotra, E. J. Murphy, and F. Walter, Astrophys. J. **656**, 770 (2007).
[9]S. Kwok and Y. Zhang, Nature **479**, 80 (2011).
[10]A. Li, Nat. Astron. **4**, 339 (2020).
[11]B. A. McGuire, R. A. Loomis, A. M. Burkhardt, K. L. K. Lee, C. N. Shingledecker, S. B. Charnley, I. R. Cooke, M. A. Cordiner, E. Herbst, S. Kalenskii, M. A. Siebert, E. R. Willis, C. Xue, A. J. Remijan, and M. C. McCarthy, Science **371**, 1265 (2021).
[12]M. Rapacioli, F. Calvo, C. Joblin, P. Parneix, D. Toublanc, and F. Spiegelman, Astron. Astrophys. **460**, 519 (2006).
[13]J. Montillaud, C. Joblin, and D. Toublanc, Astron. Astrophys. **552**, A15 (2013).
[14]M. Chabot, K. Béroff, E. Dartois, T. Pino, and M. Godard, Astrophys. J. **888**, 17 (2019).
[15]M. H. Stockett, J. N. Bull, H. Cederquist, S. Indrajith, M. Ji, J. E. Navarro Navarrete, H. T. Schmidt, H. Zettergren, and B. Zhu, Nat. Comm. 10.1038/s41467-023-36092-0 (2023).
[16]A. M. Burkhardt, K. L. K. Lee, P. B. Changala, C. N. Shingledecker, I. R. Cooke, R. A. Loomis, H. Wei, S. B. Charnley, E. Herbst, M. C. McCarthy, and B. A. McGuire, Astrophys. J. Lett. **913**, L18 (2021).
[17]L. Verstraete, EAS Publications Series **46**, 415 (2011).
[18]E. L. O. Bakes and A. G. G. M. Tielens, Astrophys. J. **427**, 822 (1994).
[19]J. C. Weingartner and B. T. Draine, Astrophys. J. Supp. Ser. **134**, 263 (2001).
[20]I. Kamp and C. P. Dullemond, Astrophys. J. **615**, 991 (2004).
[21]E. Heilbronner, P. A. Plattner, and K. Wieland, Experientia **3**, 70 (1947).
[22]M. S. Mirzaei, A. A. Taherpour, and C. Wentrup, J. Org. Chem. **87**, 3296 (2022).
[23]W. Cui, B. Hadas, B. Cao, and C. Lifshitz, J. Phys. Chem. A **104**, 6339 (2000).
[24]L. Zhao, R. Lian, I. A. Shkrob, R. A. Crowell, S. Pommeret, E. L. Chronister, A. D. Liu, and A. D. Trifunac, J. Phys. Chem. A **108**, 25 (2003).
[25]G. Reitsma, J. Hummert, J. Dura, V. Loriot, M. J. J. Vrakking, F. Lépine, and O. Kornilov, J. Phys. Chem. A **123**, 3068 (2019).
[26]J. W. L. Lee, D. S. Tikhonov, P. Chopra, S. Maclot, A. L. Steber, S. Gruet, F. Allum, R. Boll, X. Cheng, S. Düsterer, B. Erk, D. Garg, L. He, D. Heathcote, M. Johny, M. M. Kazemi, H. Köckert, J. Lahl, A. K. Lemmens, D. Loru, R. Mason, E. Müller, T. Mullins, P. Olshin, C. Passow, J. Peschel, D. Ramm, D. Rompotis, N. Schirmel, S. Trippel, J. Wiese, F. Ziaee, S. Bari, M. Burt, J. Küpper, A. M. Rijs, D. Rolles, S. Techert, P. Eng-Johnsson, M. Brouard, C. Vallance, B. Manschwetus, and M. Schnell, Nat. Comm. **12**, 6107 (2021).
[27]R. Stolze and H. Budzikiewicz, Monatsh. Chem. **109**, 325 (1978).
[28]H. Jochims, H. Rasekh, E. Rühl, H. Baumgärtel, and S. Leach, Chem. Phys. **168**, 159 (1992).

[29]K. Schroeter, D. Schröder, and H. Schwarz, J. Phys. Chem. A **103**, 4174 (1999).
[30]B. West, C. Joblin, V. Blanchet, A. Bodi, B. Sztáray, and P. M. Mayer, J. Phys. Chem. A **116**, 10999 (2012).
[31]J. Bouwman, A. J. de Haas, and J. Oomens, Chem. Comm. **52**, 2636 (2016).
[32]U. Jacovella, C. Rossi, C. Romanzin, C. Alcaraz, and R. Thissen, ChemPhysChem **24**, e202200474 (2023).
[33]G. Koster, J. M. L. Martin, and C. Lifshitz, J. Chem. Soc. Perkin Trans. 2 , 2383 (1999).
[34]Y. A. Dyakov, C.-K. Ni, S. H. Lin, Y. T. Lee, and A. M. Mebel, Phys. Chem. Chem. Phys. **8**, 1404 (2006).
[35]Y. A. Dyakov, A. M. Mebel, S. H. Lin, Y. T. Lee, and C.-K. Ni, J. Chinese Chem. Soc. **53**, 161 (2006).
[36]E. A. Solano and P. M. Mayer, J. Chem. Phys. **143**, 104305 (2015).
[37]J. Bernard, L. Chen, R. Brédy, M. Ji, C. Ortéga, J. Matsumoto, and S. Martin, Nucl. Instrum. Meth. Phys. Res. B **408**, 21 (2017).
[38]J. N. Bull, M. S. Scholz, E. Carrascosa, M. K. Kristiansson, G. Eklund, N. Punnakayathil, N. de Ruette, H. Zettergren, H. T. Schmidt, H. Cederquist, and M. H. Stockett, J. Chem. Phys. **151**, 114304 (2019).
[39]A. Nitzan and J. Jortner, J. Chem. Phys. **71**, 3524 (1979).
[40]A. Léger, P. Boissel, and L. d'Hendecourt, Phys. Rev. Lett. **60**, 921 (1988).
[41]M. Saito, H. Kubota, K. Yamasa, K. Suzuki, T. Majima, and H. Tsuchida, Phys. Rev. A **102**, 012820 (2020).
[42]A. K. Lemmens, D. B. Rap, J. M. M. Thunnissen, B. Willemsen, and A. M. Rijs, Nat. Comm. **11**, 269 (2020).
[43]H. T. Schmidt, H. A. Johansson, R. D. Thomas, W. D. Geppert, N. Haag, P. Reinhed, S. Rosén, M. Larsson, H. Danared, K.-G. Rensfelt, L. Liljeby, L. Bagge, M. Björkhage, M. Blom, P. Löfgren, A. Källberg, A. Simonsson, A. Paál, H. Zettergren, and H. Cederquist, Int. J. Astrobio. **7**, 205 (2008).
[44]H. Kreckel, O. Novotný, and A. Wolf, Phil. Trans. Roy. Soc. A **377**, 20180412 (2019).
[45]H. T. Schmidt, R. D. Thomas, M. Gatchell, S. Rosén, P. Reinhed, P. Löfgren, L. Brännholm, M. Blom, M. Björkhage, E. Bäckström, J. D. Alexander, S. Leontein, D. Hanstorp, H. Zettergren, L. Liljeby, A. Källberg, A. Simonsson, F. Hellberg, S. Mannervik, M. Larsson, W. D. Geppert, K. G. Rensfelt, H. Danared, A. Paál, M. Masuda, P. Halldén, G. Andler, M. H. Stockett, T. Chen, G. Källersjö, J. Weimer, K. Hansen, H. Hartman, and H. Cederquist, Rev. Sci. Instrum. **84**, 055115 (2013).
[46]S. Rosén, H. T. Schmidt, P. Reinhed, D. Fischer, R. D. Thomas, H. Cederquist, L. Liljeby, L. Bagge, S. Leontein, and M. Blom, Rev. Sci. Instrum. **78**, 113301 (2007).
[47]F. Salama and L. J. Allamandola, J. Chem. Phys. **94**, 6964 (1991).
[48]T. Pino, N. Boudin, and P. Bréchignac, J. Chem. Phys. **111**, 7337 (1999).
[49]J.-D. Chai and M. Head-Gordon, Phys. Chem. Chem. Phys. **10**, 6615 (2008).
[50]T. H. Dunning, J. Chem. Phys. **90**, 1007 (1989).
[51]J. A. Pople, M. Head-Gordon, and K. Raghavachari, J. Chem. Phys. **87**, 5968 (1987).
[52]M. J. Frisch, G. W. Trucks, H. B. Schlegel, G. E. Scuseria, M. A. Robb, J. R. Cheeseman, G. Scalmani, V. Barone, B. Mennucci, G. A. Petersson, H. Nakatsuji, M. Caricato, X. Li, H. P. Hratchian, A. F. Izmaylov, J. Bloino, G. Zheng, J. L. Sonnenberg, M. Hada, M. Ehara, K. Toyota, R. Fukuda, J. Hasegawa, M. Ishida, T. Nakajima, Y. Honda, O. Kitao, H. Nakai, T. Vreven, J. A. Montgomery, Jr., J. E. Peralta, F. Ogliaro, M. Bearpark, J. J. Heyd, E. Brothers, K. N. Kudin, V. N. Staroverov, R. Kobayashi, J. Normand, K. Raghavachari, A. Rendell, J. C. Burant, S. S. Iyengar, J. Tomasi, M. Cossi, N. Rega, J. M. Millam, M. Klene, J. E. Knox, J. B. Cross, V. Bakken, C. Adamo, J. Jaramillo, R. Gomperts, R. E. Stratmann, O. Yazyev, A. J. Austin, R. Cammi, C. Pomelli, J. W. Ochterski, R. L. Martin, K. Morokuma, V. G. Zakrzewski, G. A. Voth, P. Salvador, J. J. Dannenberg, S. Dapprich, A. D. Daniels, Ö. Farkas, J. B. Foresman, J. V. Ortiz, J. Cioslowski, and D. J. Fox, Gaussian 16 Revision B.01, Gaussian Inc., Wallingford CT 2016.
[53]T. M. Henderson, A. F. Izmaylov, G. Scalmani, and G. E. Scuseria, J. Chem. Phys. **131**, 044108 (2009).
[54]F. Santoro, A. Lami, R. Improta, J. Bloino, and V. Barone, J. Chem. Phys. **128**, 224311 (2008).
[55]T. Bally, C. Carra, M. P. Fülscher, and Z. Zhu, J. Chem. Soc., Perk. Trans. 2 , 1759 (1998).
[56]V. Blanchet, K. Raffael, G. Turri, B. Chatel, B. Girard, I. A. Garcia, I. Wilkinson, and B. J. Whitaker, J. Chem. Phys. **128**, 164318 (2008).
[57]M. H. Stockett, J. N. Bull, J. T. Buntine, E. Carrascosa, E. K. Anderson, M. Gatchell, M. Kaminska, R. F. Nascimento, H. Cederquist, H. T. Schmidt, and H. Zettergren, Eur. Phys. J. D **74** (2020).
[58]M. H. Stockett, J. N. Bull, J. T. Buntine, E. Carrascosa, M. Ji, N. Kono, H. T. Schmidt, and H. Zettergren, J. Chem. Phys. **153**, 154303 (2020).
[59]B. Zhu, J. N. Bull, M. Ji, H. Zettergren, and M. H. Stockett, J. Chem. Phys. **157**, 044303 (2022).
[60]K. Hansen, J. U. Andersen, P. Hvelplund, S. P. Møller, U. V. Pedersen, and V. V. Petrunin, Phys. Rev. Lett. **87**, 123401 (2001).
[61]J. U. Andersen, E. Bonderup, and K. Hansen, J. Chem. Phys. **114**, 6518 (2001).
[62]J. E. Navarro Navarrete, J. N. Bull, H. Cederquist, S. Indrajith, M. Ji, H. T. Schmidt, H. Zettergren, B. Zhu, and M. H. Stockett, Faraday Discuss. , under review (2023).
[63]S. Martin, J. Bernard, R. Brédy, B. Concina, C. Joblin, M. Ji, C. Ortega, and L. Chen, Phys. Rev. Lett. **110**, 063003 (2013).
[64]S. Martin, M. Ji, J. Bernard, R. Brédy, B. Concina, A. R. Allouche, C. Joblin, C. Ortega, G. Montagne, A. Cassimi, Y. Ngono-Ravache, and L. Chen, Phys. Rev. A **92**, 053425 (2015).
[65]J. Becker, C. Wentrup, E. Katz, and K. P. Zeller, J. Am. Chem. Soc. **102**, 5110 (1980).
[66]M. J. S. Dewar and K. M. Merz, J. Am. Chem. Soc. **108**, 5142 (1986).
[67]L. T. Scott and G. K. Agopian, J. Am. Chem. Soc. **99**, 4506 (1977).
[68]L. J. Allamandola, A. G. G. M. Tielens, and J. R. Barker, Astrophys. J. **290**, L25 (1985).
[69]L. J. Allamandola, G. G. M. Tielens, and J. R. Barker, Astrophys. J. Supp. Ser. **71**, 733 (1989).
[70]C. Joblin and A. G. G. M. Tielens, *PAHs and the Universe* (EDP Sciences, 2020).
[71]E. Peeters, S. Hony, C. V. Kerckhoven, A. G. G. M. Tielens, L. J. Allamandola, D. M. Hudgins, and C. W. Bauschlicher, Astron. Astrophys. **390**, 1089 (2002).
[72]H. Andrews, C. Boersma, M. W. Werner, J. Livingston, L. J. Allamandola, and A. G. G. M. Tielens, Astrophys. J. **807**, 99 (2015).
[73]M. J. F. Rosenberg, O. Berné, and C. Boersma, Astron. Astrophys. **566**, L4 (2014).
[74]E. Peeters, H. W. W. Spoon, and A. G. G. M. Tielens, Astrophys. J. **613**, 986 (2004).
[75]O. Berné, C. Joblin, A. Fuente, and F. Ménard, Astron. Astrophys. **495**, 827 (2009).
[76]M. C. R. Cockett, H. Ozeki, K. Okuyama, and K. Kimura, J. Chem. Phys. **98**, 7763 (1993).
[77]B. J. West, L. Lesniak, and P. M. Mayer, J. Phys. Chem. A **123**, 3569 (2019).
[78]A. Simon and M. Rapacioli, in *Chemical Modelling* (Royal Society of Chemistry) pp. 195–216.
[79]U. R. Kadhane, M. V. Vinitha, K. Ramanathan, A. S., J. Bouwman, L. Avaldi, P. Bolognesi, and R. Richter, J. Chem. Phys. **156**, 244304 (2022).
[80]K. Ramanathan, A. S., J. Bouwman, L. Avaldi, M. V. Vinitha, P. Bolognesi, R. Richter, and U. R. Kadhane, J. Chem. Phys. **157**, 064303 (2022).

[81]Y. Ling and C. Lifshitz, J. Phys. Chem. A **102**, 708 (1998).
[82]H. A. B. Johansson, H. Zettergren, A. I. S. Holm, N. Haag, S. B. Nielsen, J. A. Wyer, M.-B. S. Kirketerp, K. Støchkel, P. Hvelplund, H. T. Schmidt, and H. Cederquist, J. Chem. Phys. **135**, 084304 (2011).
[83]S. Banhatti, D. B. Rap, A. Simon, H. Leboucher, G. Wenzel, C. Joblin, B. Redlich, S. Schlemmer, and S. Brünken, Phys. Chem. Chem. Phys. **24**, 27343 (2022).
[84]A. Simon, M. Rapacioli, G. Rouaut, G. Trinquier, and F. X. Gadéa, Philos. Trans. R. Soc. A **375**, 20160195 (2017).
[85]T. Chen, Y. Luo, and A. Li, Astron. Astrophys. **633**, A103 (2020).